CHEMISTRY OF MATERIALS

pubs.acs.org/cm

Methods/Protocols

Facile Synthesis of a Library of Hollow Metallic Particles through the Galvanic Replacement of Liquid Gallium

Aleksandra S. Falchevskaya, Artur Y. Prilepskii, Sofia A. Tsvetikova, Elena I. Koshel, and Vladimir V. Vinogradov*

Cite This: *Chem. Mater.* 2021, 33, 1571−1580

Read Online

ACCESS | Metrics & More | Article Recommendations | Supporting Information

ABSTRACT: Hollow metallic capsules are of great interest given the large specific surface area and optical, electrical, and catalytic properties. To expand the possibilities of application and research of inorganic nano- and microparticles, new methodologies are being developed for obtaining metallic or multimetallic particles. For the first time, we propose a galvanic replacement reaction (GRR) with liquid gallium hydrocolloid to obtain a library of bi- and trimetallic functional capsules. The properties of the capsules are determined by the synthesis conditions, salt precursor, and stabilizer, providing control over the surface morphology and metal distribution. Furthermore, the resulting metallic capsules were tested for various functional properties, e.g., antimicrobial activity, and tailored for drug delivery systems. A wide variety of functional materials can be generated due to the ability to synthesize multimetallic capsules and incorporating a broad range of dopants.

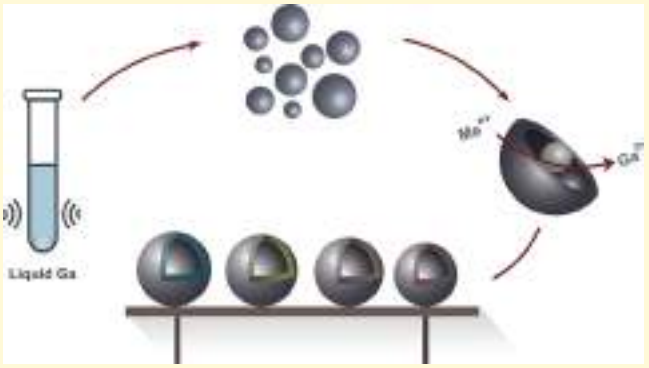

INTRODUCTION

The potential range of applications of hollow micro- and nanoparticles (HMNs) is emerging in various fields,[1] including fundamental research, drug delivery systems,[2] diagnostic imaging, catalysis,[3] nanoreactors,[4] and advanced material synthesis.[5]

Despite many existing methods of hollow nanoparticles production, their amount is significantly narrowed when it comes to purely metallic structures. First, the synthesis methods are divided into nonsolvent and solution-mediated.[6−8] The nonsolvent methods, for instance, include a spray-drying pyrolysis method when a precursor solution is sprayed on the heated surface, followed by the formation of the particles during solvent evaporation.[9] With the following method, hollow Ni nanoparticles can be produced from nickel nitrate precursor and used for CH_4 dry reforming.[10] Solution-mediated methods, in turn, are divided into template (seed-mediated) and template-free (seedless) methods.[6] The seed-mediated technique involves depositing the metals on the surface of a template made up of polymer or silica spheres followed by an etching procedure, aimed to remove the template.[11] By the mentioned method, hollow gold nanoparticles with a shell thickness of 25 nm are fabricated.[12] The main disadvantages of this method are multistage and partial destruction of the particle shell during etching. Solution-based template-free methods are more recent and are based on the preparation of hollow capsules from solid nonhollow particles. Solution-mediated methods are most suitable for the control of the capsule shape and morphology, and most importantly, they allow doping hollow capsules with additional agents, either drugs, dyes, or inks.[13,14] The Kirkendall effect is a suitable example, which involves nonequilibrium mutual diffusion of counter atoms through a reaction interface.[15] Given the mechanism of the Kirkendall effect, synthesizing hollow structures of metal oxides or sulfides is the only option; however, through repeated Kirkendall processes palladium nanocapsules with sizes of 20−26 nm were obtained, showing enhanced catalytic activity toward the oxidation of formic acid.[16]

The most suitable method of producing hollow metal structures and/or particles could be the galvanic replacement reaction (GRR). GRR is a redox process involving the oxidation of one metal, often called a sacrificial template, by ions of another metal in the solution.[17] The reaction is controlled by the difference in the standard reduction potentials of the two metal/metal ion couples involved. The first galvanic replacement reaction at the nanoscale was demonstrated with the Ag−Au system in 2002. Ag nanocubes were successfully replaced with gold via galvanic replacement

Received: October 9, 2020
Revised: February 17, 2021
Published: February 26, 2021

https://dx.doi.org/10.1021/acs.chemmater.0c03969
Chem. Mater. 2021, 33, 1571−1580

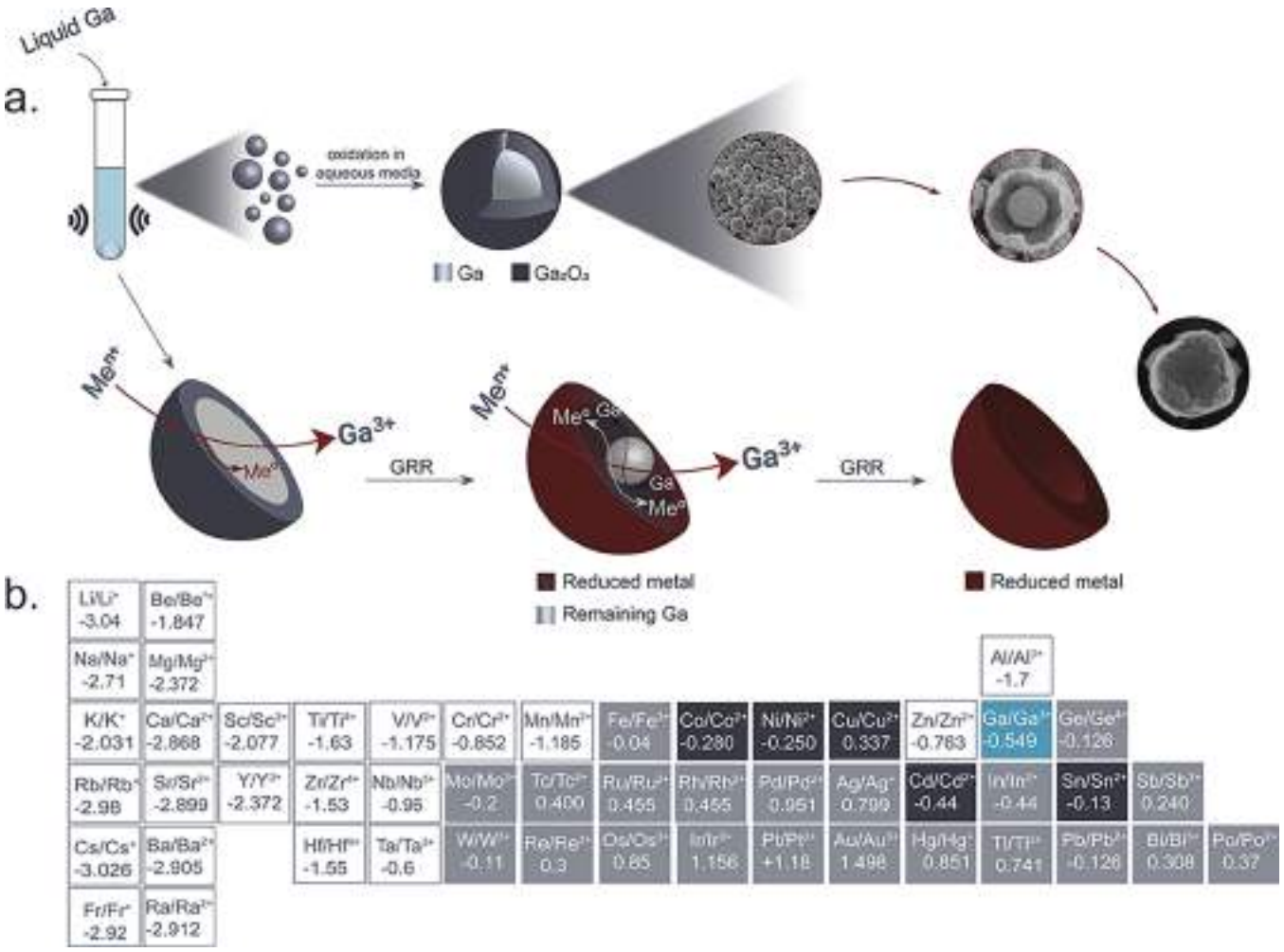

Figure 1. (a) Scheme of the galvanic replacement reaction following the formation of a hollow bimetallic sphere. It is assumed that metal salt ions (Me^{n+}) penetrate through the pores in the gallium oxide shell, gaining access to metallic gallium and initiating the galvanic replacement reaction. When gallium (Ga^{3+}) is exposed to a metal ion with a higher electrochemical potential, it oxidizes, reducing the metal ion to the metal (Me^0). (b) Periodic table: metals, highlighted in dark gray, are used for GRR in this work; in gray are metals that potentially can be involved in GRR with gallium. The rest of the shown metals cannot be used for GRR (reduction potentials of metals indicated in volts relative to the standard hydrogen electrode (SHE)).

during treatment with an $[AuCl^{4-}]$ solution.[18] Since then, many articles have been devoted to mechanistic studies of this system[19] with attention paid to the possibility of controlling the shape and morphology of the resulting nanoparticles.[20] By galvanic replacement, hollow structures or core−shell structures in the form of metal alloys can also be obtained.[21] At the same time, not enough attention has been paid to simple methods for obtaining hollow particles consisting of non-noble metals.

In the following research, the first case of the production of HMNs obtained from liquid gallium with non-noble metals using the galvanic replacement reaction as a tool is reported. The research was focused on (I) showing that a library of bi- and trimetallic capsules can be easily obtained by a newly developed template-free method during GRR with a hydrocolloid of Ga; (II) investigation of the capsule surface morphology and stability at different synthesis conditions; and (III) testing antibacterial properties and tailoring properties for drug delivery systems and other applications requiring the encapsulation of dopants.

Liquid metals have a melting point close to or below room temperature.[22] A notable feature of liquid gallium and its fusible alloys is that they are easily subjected to ultrasound, breaking into micro- and nanospheres, leading to the formation of an emulsion. It has been shown that gallium remains partially liquid at the nanoscale even when the temperature is lower than its melting point.[23] Thus, gallium micro- and nanoparticles can be obtained by melting it to a liquid state in the solvent of choice followed by an ultrasound-induced cavitation process.[24] In our case, GRR has been used for creating hollow metal capsules driven by the redox process involving the oxidation of gallium as a sacrificial template by ions of another metal in the solution. The undoubted advantage of particles from gallium and its alloys as "sacrificial" templates for GRR is that, as mentioned above, they can be obtained as a pure metal only covered with a thin oxide shell (3−10 nm)[25] and not an oxide, as in many cases.

Meanwhile, in the electrochemical series, gallium is in the position ($E^0_{Ga/Ga^{3+}} = -0.549$) where it can still be galvanically replaced by many metals (Figure 1a).[26] Therefore, it can be called a versatile template for the following reactions (Figure 1a). As illustrated in Figure 1b, many metals with an electrochemical potential higher than that of gallium can potentially participate in this reaction. Our concept has been

https://dx.doi.org/10.1021/acs.chemmater.0c03969
Chem. Mater. 2021, 33, 1571−1580

proven on five of them: copper (Cu(II), $E^0_{Cu/Cu^{2+}} = 0.337$), nickel (Ni(II), $E^0_{Ni/Ni^{2+}} = -0.250$), cobalt (Co(II), $E^0_{Co/Co^{2+}} = -0.280$), cadmium (Cd(II), $E^0_{Cd/Cd^{2+}} = -0.440$), and tin (Sn(II−IV), $E^0_{Sn/Sn^{2+}} = -0.13$). These metals were chosen as the most suitable in terms of electrode potential, their availability, and the diversity of properties. So far, studies of the GRR at the nanoscale were mainly focused on obtaining hollow capsules from noble metals (e.g., gold, silver, platinum, and palladium).[27] However, it is worth noting, in recent years, the tendency of various studies of metal particles of non-noble metals increases, given their greater commercial availability and prevalence. For example, transition metals (Cu, Co, Ni, etc.) are of great interest in catalysis, nano-optics, plasmonics, and microelectronics.[28] Even gallium itself enables local surface plasmon resonance within the UV region due to the high free electron density.[29]

EXPERIMENTAL SECTION

Chemicals. Gallium of purity 6 N (99.9999%), copper(II) nitrate trihydrate ($Cu(NO_3)_2 \times 3H_2O$), copper(II) sulfate pentahydrate ($CuSO_4 \times 5H_2O$), copper(II) acetate monohydrate ($Cu(CO_2CH_3)_2 \times H_2O$), nickel chloride hexahydrate ($NiCl_2 \times 6H_2O$), nickel(II) acetate tetrahydrate ($Ni(Ac)_2 \times 4H_2O$), cobalt(II) nitrate hexahydrate ($Co(NO_3)_2 \times 6H_2O$), hexaamminecobalt(III) chloride ($[Co(NH_3)_6]Cl_3$), cobalt chloride hexahydrate ($CoCl_2 \times 6H_2O$), cadmium(II) sulfate ($CdSO_4 \times (8/3)H_2O$), cadmium(II) sulfate tetrahydrate ($Cd(NO_3)_2 \times 4H_2O$), tin(II) chloride pentahydrate ($SnCl_2 \times 5H_2O$), polyethylenimine (PEI, Mw ∼ 25 000), polyvinylpyrrolidone (PVP, Mw ∼ 40 000), and cetyltrimethylammonium bromide (CTAB, $[(C_{16}H_{33})N(CH_3)_3]Br$) were purchased from Sigma-Aldrich, U.S.A.. High-purity water with a resistivity of 10−15 MΩ cm was obtained from an Elix Essential 3 water purification system. All solutions were freshly prepared for immediate use in each experiment.

Synthesis of Ga Micro- and Nanoparticles. Bulk gallium was melted, and a 50 mg drop of molten gallium was placed in a 10 mL plastic tube with 10 mL of water. The tube was subjected to ultrasound in an ultrasonic bath at a power of 110 W until the complete dispersion of the metal (typically, 20−30 min for 50 mg of gallium). Smooth spherical particles were obtained. Since this procedure was carried out in water and without additional degassing procedures, gallium particles were coated with a passivating oxide film, reacting with oxygen dissolved in water.[30] All subsequent synthetic procedures were performed at 20 °C unless otherwise indicated.

Synthesis of CTAB-Stabilized Particles. To stabilize the particles, before the start of the ultrasonication procedure of molten gallium, CTAB was added to the system in an amount of 1−2% of the gallium mass. The size distribution was narrower than in the absence of CTAB.

Synthesis of GaPs with the Addition of PVP. A total of 10 mg of gallium was placed in a glass tube with a diameter of 2.27 cm and 2 mm thick walls. After adding of 2 mL of PVP water solution (Mw ∼ 40 000, 1 mg/mL) to the metal, the vessel was placed in an ultrasonic bath with the following emulsification of liquid gallium during 10 min at an ultrasound power of 110 W and a frequency of 37 kHz.

Synthesis of Ga−Cu Hollow Capsules. A total of 0.0179 g of copper sulfate was dissolved in 1 mL of water in a 1 mL Eppendorf tube (C = 0.07 M). A total of 1 mL of gallium particle hydrosol (5 mg/mL) was added to the solution described above. The reaction proceeded for 1 h while shaking at a frequency of 400 rpm. Upon progression of the reaction, the solution becomes dark red. The resulted sol was centrifuged at 6000 rpm (Eppendorf 5418R) for 5 min followed by removing the supernatant and resuspension of the precipitate in 2 mL of distilled water. This procedure was repeated five times. The resulted sol was dried under a vacuum and stored at room temperature. The final capsules were designated as Ga−Cu-1.

Effect of the Salt Precursor on Ga−Cu Hollow Capsule Morphology. The previously described protocol was changed with the only difference being that instead of copper sulfate, 0.0143 g of copper acetate (C = 0.03 M) was used. The synthesized particles possessed a rough surface morphology and were designated as Ga−Cu-2. These particles ended up not being hollow inside. To obtain hollow particles from copper acetate, salt was added in two steps. First, 0.0143 g of $Cu(Ac)_2$ was added for 1.5 h of reaction, then the particles were washed three times, and the same amount of $Cu(Ac)_2$ was added. The final capsules were designated as Ga−Cu-2′.

Effect of CTAB on Ga−Cu Hollow Capsule Morphology. All synthetic procedures were similar to those described for Ga−Cu-2 capsules except the initial Ga particles were CTAB-stabilized. The synthesized particles possessed petal-like surface morphology and were designated as Ga−Cu-2−CTAB.

Effect of PEI on the Ga−Cu Hollow Capsule Morphology. The optimal concentration of PEI was selected from the PEI:Cu^{2+} ratios 1:1, 0.5:1, and 0.25:1. According to that ratio, the calculated amount of PEI was dissolved in 2 mL of distilled water. Copper salt solutions (sulfate, nitrate, and acetate) were added to the PEI solution, while the Ga:Cu^{2+} ratios remained 1:1. Light blue solutions of copper salts turned bright blue, which indicated a complexation reaction. A total of 1 mL of gallium particles was added to the PEI:Cu^{2+} solution and placed on a shaker for 1.5 h (400 rpm). Particles were centrifugated at 6000 rpm for 5 min and washed 5 times with water. The final particles were designated as Ga−Cu-2−PEI.

Synthesis of Ga−Ni Hollow Capsules. A total of 0.017 g of $NiCl_2 \times 6H_2O$ (Ga:Ni^{2+} molar ratio = 1:1) was dissolved in 1 mL of distilled water. Next, the salt solution was added to the 1 mL of gallium particles sol (5 mg/mL) and shaken for 1−24 h (400 rpm). The same procedure was performed for $Ni(NO_3)_2$, except for the different salt amounts (0.021 g).

Effect of the Salt Precursor on the Ga−Ni Hollow Capsule Morphology. A total of 0.0357 g of $Ni(Ac)_2 \times 4H_2O$ (Ga:Ni^{2+} molar ration = 1:2) was dissolved in 1 mL of distilled water and heated to 50 °C. Next, the salt solution was added to the 1 mL of gallium particles sol (5 mg/mL) and shaken for 4 h (400 rpm). The final capsules were designated as Ga−Ni-1.

Synthesis of Ga−Sn Hollow Capsules. A total of 0.02 g $SnCl_2 \times 5H_2O$ was dissolved in concentrated hydrochloric acid (300 μL, 36.5%) and added to the 5 mg of gallium particles. Gallium particles were preliminarilyy centrifuged, so tin salt was added to the "wet" precipitate. The reaction proceeded for 30 min. The final capsules were designated as Ga−Sn.

Effect of Conversion of Aqua Ions into Ammonia Complexes. A total of 5 mg of $NiCl_2 \times 6H_2O$ was dissolved in 3 mL of water in a 15 mL plastic tube, following by the addition of the excess of concentrated ammonia solution (2 mL, 25%). The color of the solution changed from light green to bright blue due to the complexation of nickel ions into $[Ni(NH_3)_6]^{2+}$. A total of 1 mL of gallium particles (5 mg/mL)

https://dx.doi.org/10.1021/acs.chemmater.0c03969
Chem. Mater. 2021, 33, 1571−1580

was added to this solution, and the reaction proceeded for 10 min, followed by centrifugation (5 min at 6000 rpm) and washing. The final capsules were designated as Ga−Ni-2. The particles have a response to a magnetic field, which indicates the presence of nickel in their composition.

A total of 5 mg of $CoCl_2 \times 6H_2O$ was dissolved in 5 mL of water in a 15 mL plastic tube, following by the addition of the excess of concentrated ammonia solution (2 mL, 25%). The color of the solution changed from pink to brown due to the complexation of cobalt ions into $[Co(NH_3)_6]^{2+}$. A total of 1 mL of gallium particles (5 mg/mL) was added to this solution, and the reaction proceeded for 10 min, during which the particles have acquired a dark gray, almost black color. Particles were washed 5 times with centrifugation (5 min at 6000 rpm). The final capsules were designated as Ga−Co. The particles have a response to a magnetic field, which indicates the presence of cobalt in their composition.

Synthesis of Ga−Cd Particles. A total of 10 mg of $Cd(NO_3)_2 \times 6H_2O$ was dissolved in 2 mL of water in a 15 mL plastic tube, followed by the addition of the excess of concentrated ammonia solution (2 mL). First, the $Cd(OH)_2$ forms a white precipitate, which then dissolves in excess of ammonia, forming a $[Cd(NH_3)_4]^{2+}$ complex. A total of 1 mL of gallium particles (5 mg/mL) was added to this solution, and the reaction proceeded for 30 min, during which the particles acquired a light gray color. Particles were washed with centrifugation (5 min at 6000 rpm). The final capsules were designated as Ga−Cd.

Characterization. Scanning electron microscopy (SEM) images were recorded on Tescan Vega 3 SBH at accelerating voltages of 5 and 20 kV. Energy dispersive analysis was conducted with the EDX detector X-ACT from Oxford Instruments, Inc., at an accelerating voltage of 20 kV. The capsule composition was analyzed using AZtec One image processing software. X-ray diffraction data were collected using a Rigaku SmartLab 3 X-ray diffractometer (4°/min) with Co Kα (fo Ga−Cu-1 and Ga−Cu-2 particles) and Mo Kα (for all other samples) anodes; XRD data were analyzed with Match!3 software. Nitrogen sorption−desorption data along with surface area analysis, pore sizes, and pore volume were analyzed with the surface area and pore size analyzer Quantachrome NOVA 1200 e. Degassing of the samples was performed at 120 °C for 20 h before the analysis. Size distribution was determined with ImageJ image analysis software. The ζ-potential was measured on Photocor Compact Z. Ion release data were obtained with the spectrophotometer Agilent Cary 60.

Bactericidal Effect Assessment. To study the bactericidal effect of the capsules, an *Escherichia coli* Nova Blue Tc^R pBad Amp^R strain was used. All the experiments were performed in the LB medium (10 g/L tryptone, 5 g/L yeast extract, 5 g/L NaCl, pH = 6.5) with ampicillin (200 μg/mL) and tetracycline (12.5 μg/mL). Overnight cultures were used for analysis. For the turbidity measurement, a culture was diluted to obtain 10^6 cells/mL and mixed with the same volume of the LB medium with antibiotics and capsules. Capsules were sterilized before the experiment with ethanol (95%) and resuspended in deionized water (concentration 4 mg/mL). The capsules were investigated at final concentrations of 200 and 400 μg/mL. Cultivation was performed at 37 °C with shaking (230 rpm) for 24 h. After that, an optical densities of the bacterial cultures (positive control), cultures with capsules (test samples), and medium without culture but with capsules were measured at 600 nm on the spectrophotometer. To calculate the optical density of bacteria, the optical density of capsules in media was subtracted from the culture optical density. Mean values and standard deviations were calculated for each concentration of the capsules. For the agar diffusion test, drops of the capsule suspension (5 μL) at a concentration 4 mg/mL were added to the bacterial lawn on the LB agar. After incubation (37 °C, 18 h), zones of the growth inhibition were analyzed. The experiments were repeated no less than three times.

Ion Release Assessment. The analysis methodology was adapted from Wen et al.[31] The same samples that were used for additional biological assessments were diluted with water to final concentrations of 200 μg/mL and 400 μg/mL, followed by the incubation of samples at 37 °C for 24 h. Thereafter, the particles were separated by centrifugation. A total of 200 μL of PEI was added to 8 mL of the supernatant. The absorption peak at 275 nm was measured on a spectrophotometer, and each experiment was repeated no less than three times.

RESULTS AND DISCUSSION

Gallium forms micro- and nanoparticles in water upon ultrasonication, yielding an emulsion. Ga particles are oxidized in water; however, the oxide shell (Ga_2O_3) does not passivate against further reaction.[32] Presumably, the formation of hollow metallic capsules during galvanic replacement reaction of Ga occurs as follows (Figure 1a). In the first stage, metal cations from the salt precursors deposit on the surface of the Ga particles and penetrate the particle through the oxide shell (3−10 nm in thickness).[25] On the second stage, metal ions are reduced, while forming the alloy/intermetallic compound particle outer layer. In the last stage, liquid Ga diffuses to the surface layer from inside to participate in GRR, thus forming a cavity. Changes in the synthesis procedure or the precursor often led to a change in morphology, as well as in the robustness of the resulting particles—they became less dense and more fragile since the shell thickness and density strongly affect their deformability.

The redox reaction includes oxidation of gallium on the anode:

$$Ga(s) \rightleftharpoons Ga^{3+}(aq) + 3e^- \quad (-0.549\ V\ vs\ SHE) \tag{1}$$

Metal reduction on the cathode is as follows:

$$Me^{n+}(aq) + ne^- \rightleftharpoons Me(s) \quad (>-0.549\ V\ vs\ SHE) \tag{2}$$

Combined, these are as follows:

$$Ga(s) + \frac{3}{n}Me^{n+}(aq) \rightleftharpoons Ga^{3+}(aq) + \frac{3}{n}Me(s) \tag{3}$$

This way, hollow bimetallic capsules were obtained by mixing different amounts of suitable salts with gallium particles in aqueous media. After each synthesis procedure, the resulted suspension was washed with water several times to ensure the absence of the salts on the surface of the obtained capsules. In our work, we were able to obtain hollow metallic capsules based on Ga with Cu, Ni, Cd, Co, and Sn (designated for the sake of brevity as Ga−Me, respectively) as well as trimetallic Ga−Cu−Ni capsules. Distinctive attention was paid to copper-containing capsules, as copper is a well-known antimicrobial agent and is used for catalysis.[33,34]

To examine the obtained capsules, scanning electron microscopy (SEM) alongside energy dispersive X-ray (EDX)

https://dx.doi.org/10.1021/acs.chemmater.0c03969
Chem. Mater. 2021, 33, 1571−1580

analysis for elemental composition recognition was used (Figure 2). SEM images of the initial gallium particles are

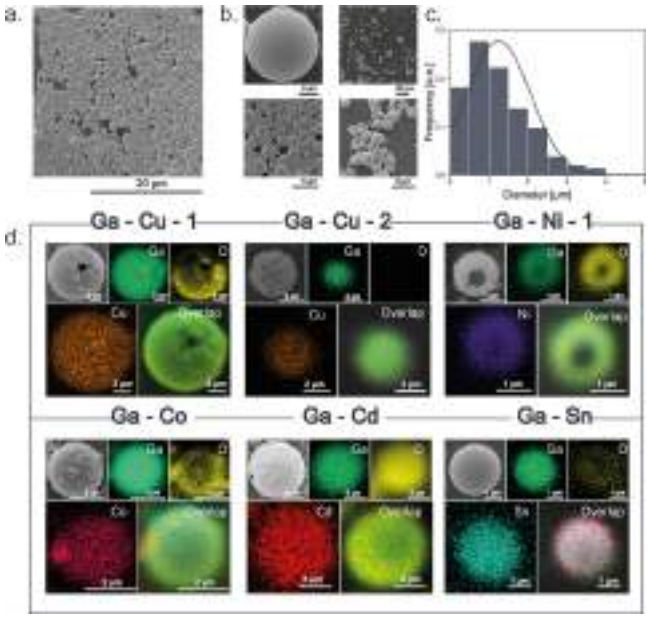

Figure 2. Structural characterization of obtained particles. (a) SEM and (b) HRSEM images of liquid gallium particles before GRR. (c) Ga particle size distribution. (d) SEM images and EDX mapping of capsules obtained after galvanic Ga0 replacement: Ga−Cu-1, Ga−Cu-2, Ga−Ni-1, Ga−Co, Ga−Cd, and Ga−Sn (see Table S1 for details of the synthesis conditions).

presented in Figure 2a. At the high-resolution SEM image (Figure 2b), it is seen that pure Ga particles have a smooth surface texture and an average size of about 1−2 μm (Figure 2c). Figure 2c shows that the Ga particles have a wide size distribution. We associate this with poor ultrasound cavitation efficiency in a plastic tube. It is known that ultrasound speed in glass is twice higher than in plastic.[35] Also, dissipation of the ultrasound energy in glass is lower than in plastic, thus providing a more uniform distribution of ultrasound waves in the sample volume.[36] Using glass tubes instead of plastic (other things being equal), we obtained particles with a narrower size distribution, with a prevalence of submicrometer particles (Figure S2a). We also used PVP to increase the stability and decrease the size distribution according to previous research.[37] Using PVP, we reduced the size distribution and shifted it to the smaller particles (Figure S2b). The use of CTAB also helps to narrow down the distribution (Figure S2c). It is important to note that GRR should be performed only with freshly prepared particles. Ga particles tend to oxidize with changing morphology (Figure S3), thus affecting GRR. More importantly, the reaction by this mechanism takes place only in the presence of a liquid template. GRR at the temperature below the Ga melting point resulted in almost zero substitution (Table S4).

At the same time, SEM images of the capsules have similar sizes but show notable differences in the surface morphology in comparison with initial Ga particles (Figure 2d). Most of the capsules are entirely closed, but some of them have an opening (shown in Figure 2d), which confirms the theory of the galvanic growth on defects.[8]

During the reaction, often due to a local excess of salt, some capsules break apart, which makes it possible to determine the approximate wall thickness (see Figure S4 for SEM images, Figure S5 for measurements details, and Table S2 for details). Wall thickness decreases with the decrease of the metal salt concentration. For Ga−Cu systems, for instance, the wall thickness lies in the range of 30−130 nm, and for Ga−Ni it is in the range of 300−500 nm. Due to the vast polydispersity of the original Ga particles, the inner volume of the resulted bimetallic capsules also varies immensely, from 1.8 to 1800 μm^3 (Table S2).

Typically, hollow particles have a much larger surface area than their nonhollow counterparts. We performed additional investigation using low-temperature nitrogen physisorption to measure the surface area and porosity of our capsules. The surface area and pore volume of the obtained capsules after the GRR increased by 4−10 times in comparison with those of gallium particles (Table S3, Figure S6).

For instance, the surface area of hollow Ga−Cu and Ga−Ni capsules increased from ~2 m^2/g (pure Ga) to 28 m^2/g and 20 m^2/g, respectively. Data from XRD analysis for synthesized capsules are shown in Figure S1, Supporting Information. In the case of Ga−Cu capsules, for both samples (Ga−Cu-1 and Ga−Cu-2), no metallic gallium remained in the system; only metallic copper and a newly formed $CuGa_2$ alloy (Figure S1a,b) were present. The phase ratios for Ga−Cu-1 were $CuGa_2$ = 70.8% and Cu = 29.2%; for Ga−Cu-2, $CuGa_2$ = 19.4% and Cu = 80.6%. All of the capsule samples were highly crystalline, and the Ga−Co capsules were the only exception, showing a partially amorphous structure (Figure S1c). A situation similar to that of Ga−Cu occurs in the gallium−nickel system (Ga−Ni-2), where the GaNi alloy is the dominant phase (Figure S1d). The formation of GaOOH is associated with a more prolonged ultrasonic dispersion of this sample, which led to overheating of the system and accelerating the oxidation of gallium. In the samples with cobalt and tin, in addition to pure metals, there were also alloys of the composition $Co_{0.92}Ga_{0.08}$ and $Sn_{0.929}Ga_{0.071}$ (5.2% and 32.8%, respectively) (Figure S1e). Finally, in the case of Cd substitution, the main components are gallium (75.8%) and cadmium (16.7%) with trace amounts of mixed oxide Ga_2CdO_4 (Figure S1f).[38−40]

Further studies were focused on the impact of the precursor, stabilizer, and reaction time on the surface morphology and stability of the resulting capsules. We initially started our investigation from copper-containing systems. Copper sulfate was taken as the first tested metal precursor. Among the studied range of copper sulfate concentrations (0.01−0.1 M), the best capsules (highest copper content and structural stability) were obtained with a salt concentration of 0.036 M and a Ga:Cu^{2+} ratio of 1:1 (Figure 3a). To examine the impact of precursors on the resulted capsules, we included copper nitrate and copper acetate into the experimental routine. While the results obtained with copper sulfate and nitrate were similar, the capsules obtained after the reaction with copper acetate under the same conditions have a rough surface morphology, remaining generally spherical (Figure 3b). Meanwhile, after the destruction of Ga−Cu-2 particles with ultrasound, it was discovered that there is no cavity inside. The outer shell of copper and gallium was filled with pure gallium (Figure 3c, inset). An additional experiment was performed, and copper acetate was added in two steps, separated by washing. It has been shown that, with this procedure, it is possible to obtain precisely hollow capsules with a smoother surface (Ca−Cu-2′, Figure 3d).

https://dx.doi.org/10.1021/acs.chemmater.0c03969
Chem. Mater. 2021, 33, 1571−1580

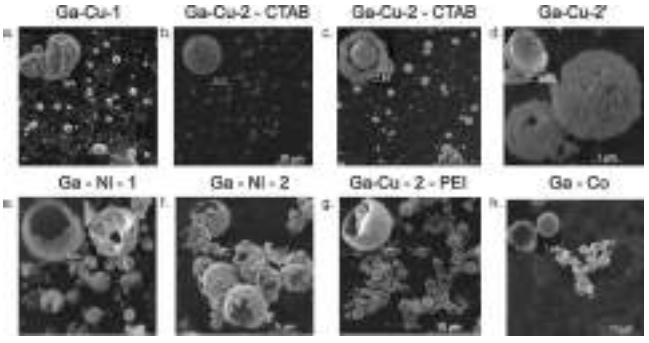

Figure 3. SEM images of synthesized capsules. (a) Ga−Cu-1 capsules; (b) Ga−Cu-2−CTAB capsules; (c) Ga−Cu-2−CTAB particles showing the inner gallium core; (d) Ga−Cu-2′ capsules obtained by two-step addition of copper acetate; (e) Ga−Ni-1 capsules; (f) Ga−Ni-2 capsules; (g) Ga−Cu-2−PEI capsules; and (h) Ga−Co capsules

To explain the above-mentioned phenomena, we need to discuss the thermodynamics of a galvanic cell. Even if $E^0(Me^{n+}/Me) \gg E^0(Ga^{3+}/Ga)$, it is measured under standard conditions and varies from the activities of the ions and temperature. The standard electrode potential for a reaction of type $aOx_1 + bRed_2 \rightleftharpoons aRed_1 + bOx_2$, related to the "real" potential by Nernst equation, is

$$E_{cell} = E^0 + \frac{RT}{nF} \ln \frac{a^b_{Ox_2} a^a_{Red_1}}{a^b_{Red_2} a^a_{Ox_1}} \quad (4)$$

where $a^{a/b}$ is the chemical activity in the degree of chemical indices, R is the universal gas constant, T is the temperature in Kelvin, n is the number of electrons transferred in the cell reaction, and F is the Faraday constant.

During the redox reaction, the concentrations of ions (and, therefore, chemical activities) in the system change dynamically. The heterogeneous reaction, such as in our case, proceeds until the redox potentials of the $E^0(Ox_1/Red_1)$ and $E^0(Ox_2/Red_2)$ (i.e., $E^0(Me^{n+}/Me)$ and $E^0(Ga^{3+}/Ga)$, respectively) couples become equal to each other.[41] Consequently, the second step reaction with the same salt allows the GRR to proceed more thoroughly without the need for high concentrations of salt, which can lead to the destruction of the capsules.

Similar experiments were conducted with the Ga−Ni system. To study the effect of the precursor, different nickel salts (namely, chloride, nitrate, and acetate) were taken. It was observed that the use of nickel chloride and nickel nitrate resulted in obtaining the capsules with approximately 0.4% of the metal nickel phase, even after 24 h of reaction, indicating a deficient degree of gallium substitution. Similar behavior was observed for cadmium and cobalt systems. On the other hand, when using nickel acetate, a better final Ga:Ni (1.6:1) ratio was obtained. However, the resulted capsules lost their spherical shape, becoming more "curved" (Figures 2d and 3e). Interestingly, a similar case was discussed previously in ref 42, where the kinetics of metals from their salts by a zinc amalgam reduction were studied. It turned out that when metal salts are converted to anionic or cationic complexes, the reaction proceeds almost instantly. The possible explanation of this effect is the steric hindrance of H_2O groups around the metal cation, which blocks valence electrons. To prove these assumptions, we converted existing ions in the initial conditions $[Ni(H_2O)_6]^{2+}$, $[Co(H_2O)_6]^{2+}$, and $[Cd(H_2O)_4]^{2+}$ into $[Ni(NH_3)_6]^{2+}$, $[Co(NH_3)_6]^{2+}$, and $[Cd(NH_3)_4]^{2+}$ by adding in a concentrated ammonia solution. This allows us to accelerate the GRR 10-fold and increase the amount of metal being replaced in the particles dramatically (Figure 3f−h, Table S2). For instance, the Ga:Ni ratio changed from 1.6:1 to 1:2.2, the Ga:Co ratio changed from 300:1 to 1:3.67, and the Ga:Cd ratio changed from 210:1 to 1:58.4.

When substituted with tin chloride, it must be kept in mind that tin chloride forms the insoluble compound Sn(OH)Cl upon dilution. To avoid this unwanted effect, the salt was dissolved in the concentrated hydrochloric acid (5 mg/mL of acid), and this solution was added to the Ga particles, avoiding dilution. The resulted capsules were smooth and spherical (Figure 2d). The gallium to tin ratio in the final sample varies from 1:9 to complete conversion to clusters of tin particles. However, it should be noted that, with full conversion, the particles are significantly destroyed, so the method could be improved in further experiments.

The reactions with copper salts are quite intense, which often leads to a high percentage of destroyed capsules with surface irregularities. We have made attempts to stabilize this system. There are two ways: to stabilize the original particles and to influence the course of the reaction itself. We studied three systems: without any additions (Ga−Cu-2), with the addition of the surfactant CTAB (Ga−Cu-2−CTAB), and with the addition of the polyelectrolyte PEI (Ga−Cu-2−PEI) (Figure 4). The initial Ga−Cu-2 system was described above

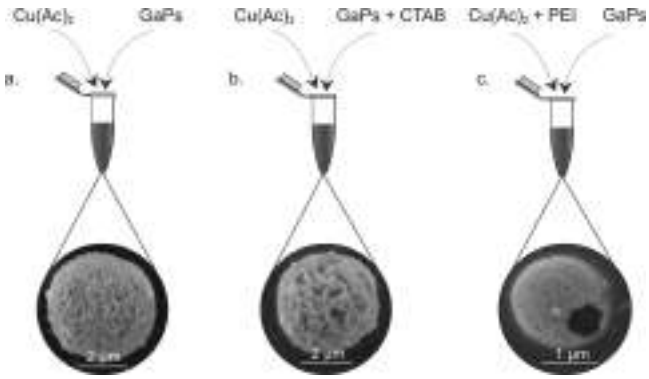

Figure 4. SEM images of Ga−Cu capsules were obtained in different conditions. (a) Capsules obtained without any stabilizers (Ga−Cu-2); (b) Ga−Cu capsules, obtained with the addition of CTAB during the synthesis of initial gallium particles; and (c) Ga−Cu capsules, obtained with the addition of PEI (Ga−Cu-2−PEI). A high degree of substitution was observed, and even full conversion to hollow copper capsules has been reached (Table S2).

and is represented in Figure 4a. The cationic surfactant CTAB was used to provide the electrostatic interaction with negatively charged Ga nanoparticles (ζ-potential = −2 mV) and therefore stabilize it.[25] It was noted that if CTAB is added during the synthesis of capsules, the final capsules look more superficially solid than the capsules obtained in the absence of a stabilizer and have a flower-like structure (Figure 4b).

There are several works on obtaining particles of copper oxide similar in morphology by precipitation or hydrothermal methods.[43−45] The precursor effect is not always clear; however, it is known that different anions can affect nucleation and crystal growth. For instance, no surfactants were used when flower-like copper oxide particles were obtained using

https://dx.doi.org/10.1021/acs.chemmater.0c03969
Chem. Mater. 2021, 33, 1571−1580

copper acetate by the precipitation method.[43] The authors state that, at the initial stages, copper oxide is released in the form of separate nanoclusters, which subsequently undergo self-organization and Ostwald ripening, forming 2D sheets.

CTAB has been also widely used in the fabrication of nanomaterials to control the morphology of copper and copper oxide nanoparticles.[46] Flower-like CuO nanostructures were formed during the CTAB-assisted hydrothermal method. In that case, authors speculate that CTAB acts as a cationic surfactant forming $CTA^{+}-[Cu(OH)_4]^{2-}$ ion pairs at the beginning of the hydrothermal process, accelerating the ionization of $[Cu(OH)_4]^{2-}$.[44] Also, it is possible to obtain copper nanotriangles.[45] The authors used CTAB to direct the growth of particles by blocking the particle surface. Moreover, the authors postulate that CTAB acts as a micrometer level micelle, guiding the growth of the irregularities. We suggest that, in the case of our GRR, both mechanisms take place, resulting in a flower morphology.

PEI was used as a cationic polyelectrolyte to see the effect of the polymer-based stabilizer. Polyethylenimine has been used because of its known ability to complex with copper cations. Thus, it was supposed to reduce the concentration of free copper aqua-complexes, providing a more uniform course of the reaction. Moreover, PEI as a viscous polymer could increase the viscosity of the medium, decreasing the reaction rate. The obtained capsules, in contrast to those obtained without stabilizer, appear to be less crumpled but, at the same time, more fragile, with thin walls and visible pores (Figures 4c and S7). Moreover, using this method, a higher degree of substitution was observed, and even full conversion to hollow copper capsules has been reached (Table S2).

When assessing the impact of the reaction time, it was observed that the resulted capsules are not as affected by it as much as they are affected by the initial concentration of the salt or the type of precursor. For instance, the time dependences of the Ga:Cu ratio for the Ga−Cu-2 system are shown in Figure S8. The GRR course for all concentrations was linear, without a significant increase in the final Ga:Cu ratio over time.

In the last round of experiments, it was interesting to determine the ability of the proposed GRR method to synthesize trimetallic capsules by conducting two galvanic replacements in a row, as described in Figure 5. The salt addition was ordered according to the electrode potentials of the following salts. For Ga−Cu−Ni capsules, copper acetate was initially added in a molar ratio of $Ga:Cu^{2+}$ as 1:0.5. First, ordinary bimetallic capsules were obtained, where one of the metals had $E^0 = -0.549$ V (gallium), and for the second metal $E^0 = 0.3419$ V (copper). Consequently, when Ni^{2+} is added, gallium rather than copper will be replaced (Figure 5). The resulting Ga:Cu:Ni ratio was 15:17:1.

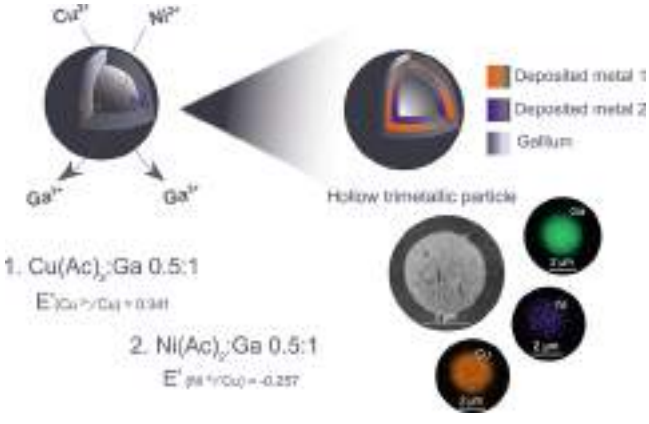

Figure 5. Scheme of trimetallic Ga−Cu−Ni capsule synthesis. Component ratio and SEM with corresponding element mapping images are shown.

It has long been established that metal and metal oxide nanoparticles have an inhibitory effect on bacteria cultures. Metal nanoparticles can exert their effect on microbial cells by generating membrane damage, oxidative stress, and damage to proteins and DNA. Hollow capsules can provide better antimicrobial activity due to the ability to encapsulate antibacterial agents. Moreover, it has been proven that bimetallic structures exhibit more significant antimicrobial activity, surpassing monometallic counterparts due to synergistic effects.[47] In some cases, synergistic activity may appear when metal and bimetal particles are doped with antibacterial agents.[48] Initially, evaluation experiments were carried out on the bacterial activity of the obtained particles.

A bactericidal effect of the capsules was tested on the *Escherichia coli* Nova Blue Tc^R pBad Amp^R at 200 and 400 μg/mL concentrations in the Lysogeny broth (LB) medium (Figure S9). In general, the antimicrobial effect for capsules is represented by the following dependency in descending order: Ga−Co ≫ Ga−Cu-2 ≫ Ga−Cd > Ga−Sn > Ga−Ni-1 > Ga−Cu-3 > Ga. The most remarkable effect was caused by Ga−Co capsules. A significant bactericidal activity at a concentration of 400 μg/mL was also revealed for the Ga−Cu-2 capsules. Other capsules have shown a slight dose-dependent effect, but an increase of the concentration may be required to reach a significant antimicrobial activity. To confirm these results, an additional inhibition zone method was carried out. A certain number of capsules were applied to a Petri dish with preseeded bacteria on agar (Figure S10). The results are in good agreement with the previous experiment. It was expected that capsules with cadmium, for example, will have the most pronounced effect, but this was not the case in the experiment. Naturally, this is directly related to the fact that, in the case of cadmium, the reaction is not as intense as, for example, with cobalt hexaaminochloride or copper salts, which ultimately result in different amounts of metals in the final capsules, which causes a difference in bactericidal effects.

The experiments show that particles of the gallium−copper composition of different morphologies have different antibacterial activities. We decided to carry out additional experiments to evaluate antimicrobial activity dependence from the morphology and the ratio of metals in the samples and correlate this with the release of copper ions from each sample. For this aim, four samples were synthesized: Ga−Cu-1 (Ga:Cu = 1:0.25), Ga−Cu-2−CTAB (Ga:Cu = 1:0.5), Ga−Cu−PEI (Ga:Cu = 1:0.25), and Ga−Cu−PEI (Ga:Cu = 1:0.5). To assess the influence of the type of capsule surface, we performed an additional CFU counting experiment (see Figure S11). In the test, we revealed that Ga−Cu-1 and Ga−Cu-2−CTAB particles have a bactericidal effect (decrease of cell number for one order), and the effect is dose-dependent. Interestingly, the ion release experiment showed (Figure S9c) no correlation between the antibacterial activity and the amount of released ions. We assume that in the case of Ga−Cu-2−CTAB particles with the rough surface the main contribution to the antibacterial effect may be connected with physical interactions. It is well-known that surface

https://dx.doi.org/10.1021/acs.chemmater.0c03969
Chem. Mater. 2021, 33, 1571−1580

roughness can affect the antibacterial properties of inorganic particles.[49−51] The main mechanisms were connected with the physical interaction of nanoparticles with bacterial shells causing direct damage and disturbances in the membrane structure and cell metabolism. Further investigation would be focused on organically doped capsules, as they are known to lead to synergistic effects.[48]

CONCLUSIONS

A universal methodology was proposed to generate hollow metallic micro- and nanoparticles from liquid gallium, based on versatile GRR in an aqueous environment. Several metals were incorporated into the walls of the particles, leaving the hollow gap replacing liquid gallium. The hollowing degree, the reaction intensity, and the morphology of resulted capsules, as well as the wall thickness thereof, can be controlled by the reaction time, amounts of reagents, and surfactant addition. Metallic capsules showed promising antibacterial properties that will be further investigated after encapsulation with organic molecules for tailoring bifunctional antibacterial drug delivery systems. The ability to obtain a wide range of multimetallic capsules and to incorporate a variety of dopants opens a new promising synthetic direction for functional materials production.

ASSOCIATED CONTENT

Supporting Information

The Supporting Information is available free of charge at https://pubs.acs.org/doi/10.1021/acs.chemmater.0c03969.

Table S1, general synthetic methods for bimetallic capsules; Table S2, the effect of precursors on wall thickness; Table S3, N_2 adsorption−desorption data; Table S4, GRR effectiveness at different temperatures in terms of Ga:Cu ratio in Ga−Cu samples; Figure S1, X-ray diffraction data; Figure S2, size distribution of particles obtained by different procedures; Figure S3, oxidation of particles over time; Figure S4, SEM images of destroyed capsules; Figure S5, wall thickness determination of the obtained capsules; Figure S6, nitrogen adsorption−desorption isotherms and BJH pore-size distributions; Figure S7, large-scale production images; Figure S8, the ratio of Ga:Cu in final Ga−Cu-2 capsules versus reaction time and initial concentrations of $Cu(Ac)_2$; and Figure S9, the antibacterial activity of capsules against *Escherichia coli* measured by different methods (PDF)

AUTHOR INFORMATION

Corresponding Author

Vladimir V. Vinogradov − *ITMO University, International Institute "Solution Chemistry of Advanced Materials and Technologies" (SCAMT), Saint Petersburg 191002, Russian Federation;* orcid.org/0000-0002-5081-4876; Email: vinogradov@scamt-itmo.ru

Authors

Aleksandra S. Falchevskaya − *ITMO University, International Institute "Solution Chemistry of Advanced Materials and Technologies" (SCAMT), Saint Petersburg 191002, Russian Federation*

Artur Y. Prilepskii − *ITMO University, International Institute "Solution Chemistry of Advanced Materials and Technologies" (SCAMT), Saint Petersburg 191002, Russian Federation;* orcid.org/0000-0003-0539-6545

Sofia A. Tsvetikova − *ITMO University, International Institute "Solution Chemistry of Advanced Materials and Technologies" (SCAMT), Saint Petersburg 191002, Russian Federation*

Elena I. Koshel − *ITMO University, International Institute "Solution Chemistry of Advanced Materials and Technologies" (SCAMT), Saint Petersburg 191002, Russian Federation;* orcid.org/0000-0002-8957-5956

Complete contact information is available at: https://pubs.acs.org/10.1021/acs.chemmater.0c03969

Author Contributions

A.S.F. performed the synthesis of particles and wrote the original manuscript; A.Y.P. wrote the original manuscript and edited the manuscript; S.A.T. performed the experiments with the bacterial cultures; E.I.K. performed the experiments with bacterial cultures; and V.V.V. supervised the entire work and edited the manuscript.

Funding

The work was supported by the Ministry of Science and Higher Education of the Russian Federation (Project No.075-15-2019-1896). The work of A.S.F. and A.Y.P. was supported by the Ministry of Science and Higher Education of the Russian Federation grant number MK-1389.2020.3.

Notes

The authors declare no competing financial interest.

ACKNOWLEDGMENTS

The X-ray powder diffraction studies were performed on the Rigaku SmartLab 3 diffractometer of the Saint-Petersburg State Technological Institute (Technical University). The authors thank Sviatlana A. Ulasevich for help in the field of sonochemistry and Elizaveta Gusarova for assistance.

REFERENCES

(1) Wang, X.; Feng, J.; Bai, Y.; Zhang, Q.; Yin, Y. Synthesis, Properties, and Applications of Hollow Micro-/Nanostructures. *Chem. Rev.* **2016**, *116* (18), 10983−11060.

(2) Ren, N.; Wang, B.; Yang, Y. H.; Zhang, Y. H.; Yang, W. L.; Yue, Y. H.; Gao, Z.; Tang, Y. General Method for the Fabrication of Hollow Microcapsules with Adjustable Shell Compositions. *Chem. Mater.* **2005**, *17* (10), 2582−2587.

(3) Li, B.; Zeng, H. C. Architecture and Preparation of Hollow Catalytic Devices. *Adv. Mater.* **2019**, *31* (38), 1801104.

(4) Zhu, W.; Chen, Z.; Pan, Y.; Dai, R.; Wu, Y.; Zhuang, Z.; Wang, D.; Peng, Q.; Chen, C.; Li, Y. Functionalization of Hollow Nanomaterials for Catalytic Applications: Nanoreactor Construction. *Adv. Mater.* **2019**, *31* (38), 1800426.

(5) Rahman, M. M.; Elaissari, A. A Versatile Method for the Preparation of Rigid Submicron Hollow Capsules Containing a Temperature Responsive Shell. *J. Mater. Chem.* **2012**, *22* (3), 1173−1179.

(6) Fuji, M.; Han, Y. S.; Takai, C. Synthesis and Applications of Hollow Particles. *KONA* **2013**, *30* (30), 47−68.

(7) Soares, S. F.; Fernandes, T.; Daniel-Da-Silva, A. L.; Trindade, T. The Controlled Synthesis of Complex Hollow Nanostructures and Prospective Applications. *Proc. R. Soc. London, Ser. A* **2019**, *475* (2224), 20180677.

(8) Feng, J.; Yin, Y. Self-Templating Approaches to Hollow Nanostructures. *Adv. Mater.* **2019**, *31* (38), 1802349.

(9) Eslamian, M.; Ashgriz, N. Handbook of Atomization and Sprays; Springer Science & Business Media: 2011; pp 849−860.

(10) Aghaali, M. H.; Firoozi, S. Synthesis of Nanostructured Fcc/Hcp Hollow Ni Particles by Ultrasonic Spray Pyrolysis and Its Dry Reforming Catalytic Properties. *Powder Technol.* **2019**, *356*, 119−128.
(11) Liu, R.; Yang, S.; Wang, F.; Lu, X.; Yang, Z.; Ding, B. Sodium Chloride Template Synthesis of Cubic Tin Dioxide Hollow Particles for Lithium Ion Battery Applications. *ACS Appl. Mater. Interfaces* **2012**, *4* (3), 1537−1542.
(12) Abdollahi, S. N.; Naderi, M.; Amoabediny, G. Synthesis and Characterization of Hollow Gold Nanoparticles Using Silica Spheres as Templates. *Colloids Surf., A* **2013**, *436*, 1069−1075.
(13) Jiu, H.; Jia, W.; Zhang, L.; Huang, C.; Jiao, H.; Chang, J. Synthesis, Luminescent and Drug-Release Properties of SiO2@ Y2O3:Eu Hollow Mesoporous Microspheres. *J. Porous Mater.* **2015**, *22* (6), 1511−1518.
(14) Mosquera, J.; Szyszko, B.; Ho, S. K. Y.; Nitschke, J. R. Sequence-Selective Encapsulation and Protection of Long Peptides by a Self-Assembled Fe II 8 L 6 Cubic Cage. *Nat. Commun.* **2017**, *8*, 6−11.
(15) Yin, Y.; Rioux, R. M.; Erdonmez, C. K.; Hughes, S.; Somorjal, G. A.; Alivisatos, A. P. Formation of Hollow Nanocrystals Through the Nanoscale Kirkendall Effect. *Science (Washington, DC, U. S.)* **2004**, *304* (5671), 711−714.
(16) Tianou, H.; Wang, W.; Yang, X.; Cao, Z.; Kuang, Q.; Wang, Z.; Shan, Z.; Jin, M.; Yin, Y. Inflating Hollow Nanocrystals through a Repeated Kirkendall Cavitation Process. *Nat. Commun.* **2017**, *8* (1), 1261.
(17) El Mel, A. A.; Chettab, M.; Gautron, E.; Chauvin, A.; Humbert, B.; Mevellec, J. Y.; Delacote, C.; Thiry, D.; Stephant, N.; Ding, J.; et al. Galvanic Replacement Reaction: A Route to Highly Ordered Bimetallic Nanotubes. *J. Phys. Chem. C* **2016**, *120* (31), 17652−17659.
(18) Sun, Y.; Xia, Y. Shape-Controlled Synthesis of Gold and Silver Nanoparticles. *Science (Washington, DC, U. S.)* **2002**, *298* (5601), 2176−2179.
(19) Cobley, C. M.; Xia, Y. Engineering the Properties of Metal Nanostructures via Galvanic Replacement Reactions. *Mater. Sci. Eng., R* **2010**, *70* (3−6), 44−62.
(20) Da Silva, A. G. M.; Rodrigues, T. S.; Haigh, S. J.; Camargo, P. H. C. Galvanic Replacement Reaction: Recent Developments for Engineering Metal Nanostructures towards Catalytic Applications. *Chem. Commun.* **2017**, *53*, 7135−7148.
(21) He, W.; Wu, X.; Liu, J.; Hu, X.; Zhang, K.; Hou, S.; Zhou, W.; Xie, S. Design of AgM Bimetallic Alloy Nanostructures (M = Au, Pd, Pt) with Tunable Morphology and Peroxidase-like Activity. *Chem. Mater.* **2010**, *22* (9), 2988−2994.
(22) Song, H.; Kim, T.; Kang, S.; Jin, H.; Lee, K.; Yoon, H. J. Ga-Based Liquid Metal Micro/Nanoparticles: Recent Advances and Applications. *Small* **2020**, *16* (12), 1903391.
(23) Kumar, V. B.; Koltypin, Y.; Gedanken, A.; Porat, Z. Ultrasonic Cavitation of Molten Gallium in Water: Entrapment of Organic Molecules in Gallium Microspheres. *J. Mater. Chem. A* **2014**, *2* (5), 1309−1317.
(24) Kumar, V. B.; Gedanken, A.; Kimmel, G.; Porat, Z. Ultrasonic Cavitation of Molten Gallium: Formation of Micro- and Nano-Spheres. *Ultrason. Sonochem.* **2014**, *21* (3), 1166−1173.
(25) Lin, Y.; Liu, Y.; Genzer, J.; Dickey, M. D. Shape-Transformable Liquid Metal Nanoparticles in Aqueous Solution. *Chem. Sci.* **2017**, *8* (5), 3832−3837.
(26) Lide, D. R. *Handbook of Chemistry and Physics*, 84th ed.; CRC Press: 2004; pp 1217−1222.
(27) Xia, X.; Wang, Y.; Ruditskiy, A.; Xia, Y. 25th Anniversary Article: Galvanic Replacement: A Simple and Versatile Route to Hollow Nanostructures with Tunable and Well-Controlled Properties. *Adv. Mater.* **2013**, *25* (44), 6313−6333.
(28) Kim, S.; Kim, J. M.; Park, J. E.; Nam, J. M. Nonnoble-Metal-Based Plasmonic Nanomaterials: Recent Advances and Future Perspectives. *Adv. Mater.* **2018**, *30*, 1704528.
(29) Wu, P. C.; Losurdo, M.; Kim, T. H.; Giangregorio, M.; Bruno, G.; Everitt, H. O.; Brown, A. S. Plasmonic Gallium Nanoparticles on Polar Semiconductors: Interplay between Nanoparticle Wetting, Localized Surface Plasmon Dynamics, and Interface Charge. *Langmuir* **2009**, *25* (2), 924−930.
(30) Lin, Y.; Genzer, J.; Li, W.; Qiao, R.; Dickey, M. D.; Tang, S. Y. Sonication-Enabled Rapid Production of Stable Liquid Metal Nanoparticles Grafted with Poly(1-Octadecene-: Alt -Maleic Anhydride) in Aqueous Solutions. *Nanoscale* **2018**, *10* (42), 19871−19878.
(31) Wen, T.; Qu, F.; Li, N. B.; Luo, H. Q. A Facile, Sensitive, and Rapid Spectrophotometric Method for Copper(II) Ion Detection in Aqueous Media Using Polyethyleneimine. *Arabian J. Chem.* **2017**, *10* (Ii), S1680−S1685.
(32) Creighton, M. A.; Yuen, M. C.; Susner, M. A.; Farrell, Z.; Maruyama, B.; Tabor, C. E. Oxidation of Gallium-Based Liquid Metal Alloys by Water. *Langmuir* **2020**, *36* (43), 12933−12941.
(33) Ramyadevi, J.; Jeyasubramanian, K.; Marikani, A.; Rajakumar, G.; Rahuman, A. A. Synthesis and Antimicrobial Activity of Copper Nanoparticles. *Mater. Lett.* **2012**, *71*, 114−116.
(34) Kumar, V.; Mohapatra, T.; Dharmadhikari, S.; Ghosh, P. A Review Paper on Heterogeneous Fenton Catalyst: Types of Preparation, Modification Techniques, Factors Affecting the Synthesis, Characterization, and Application in the Wastewater Treatment. *Bull. Chem. React. Eng. Catal.* **2020**, *15* (1), 1−34.
(35) Laugier, P.; Haïat, G. *Bone Quantitative Ultrasound*; Springer: Dordrecht, 2011; pp 29−45.
(36) Canselier, J. P.; Delmas, H.; Wilhelm, A. M.; Abismaïl, B. Ultrasound Emulsification - An Overview. *J. Dispersion Sci. Technol.* **2002**, *23* (1−3), 333−349.
(37) Liu, Y.; Wang, Q.; Bi, S.; Zhang, W.; Zhou, H.; Jiang, X. Water-Processable Liquid Metal Nanoparticles by Single-Step Polymer Encapsulation. *Nanoscale* **2020**, *12* (25), 13731−13741.
(38) Villars, P.; Cenzual, K.; Gladyshevskii, R. *Handbook*; Walter de Gruyter GmbH & Co KG: 2014; pp 93−97.
(39) Liu, S.; Qu, D.; McDonald, S.; Gu, Q.; Matsumura, S.; Nogita, K. Intermetallic Formation Mechanisms and Properties in Room-Temperature Ga Soldering. *J. Alloys Compd.* **2020**, *826*, 154221.
(40) Xiong, M.; Gao, Y.; Liu, J. Fabrication of Magnetic Nano Liquid Metal Fluid through Loading of Ni Nanoparticles into Gallium or Its Alloy. *J. Magn. Magn. Mater.* **2014**, *354*, 279−283.
(41) Seeber, R.; Zanardi, C.; Inzelt, G. Links between Electrochemical Thermodynamics and Kinetics. *ChemTexts* **2015**, *1* (4), 18.
(42) Russell, A. S.; Carver, J. C. (Dr. L. L. Reduction of Ions of Nickel, Cobalt, Iron and Other Metals by Zinc Amalgam [5]. *Nature* **1938**, *142* (3587), 210−211.
(43) Wang, X.; Yang, J.; Shi, L.; Gao, M. Surfactant-Free Synthesis of CuO with Controllable Morphologies and Enhanced Photocatalytic Property. *Nanoscale Res. Lett.* **2016**, *11* (1), 125.
(44) Zou, Y.; Li, Y.; Zhang, N.; Li, J. Prepared of Flower-like CuO via CTAB-Assisted Hydrothermal Method. *Adv. Mater. Res.* **2010**, *152−153*, 909−914.
(45) Wang, J.; Guo, X.; He, Y.; Jiang, M.; Sun, R. The Synthesis and Tribological Characteristics of Triangular Copper Nanoplates as a Grease Additive. *RSC Adv.* **2017**, *7* (64), 40249−40254.
(46) Chen, L.; Zhang, D.; Chen, J.; Zhou, H.; Wan, H. The Use of CTAB to Control the Size of Copper Nanoparticles and the Concentration of Alkylthiols on Their Surfaces. *Mater. Sci. Eng., A* **2006**, *415*, 156.
(47) Arora, N.; Thangavelu, K.; Karanikolos, G. N. Bimetallic Nanoparticles for Antimicrobial Applications. *Front. Chem.* **2020**, *8* (May), 1−22.
(48) Bauer, T. S.; Menagen, B.; Avnir, D.; Hayouka, Z. Random Peptide Mixtures Entrapped within a Copper-Cuprite Matrix: New Antimicrobial Agent against Methicillin-Resistant Staphylococcus Aureus. *Sci. Rep.* **2019**, *9* (1), 11215.
(49) Sirelkhatim, A.; Mahmud, S.; Seeni, A.; Kaus, N. H. M.; Ann, L. C.; Bakhori, S. K. M.; Hasan, H.; Mohamad, D. Review on Zinc Oxide Nanoparticles: Antibacterial Activity and Toxicity Mechanism. *Nano-Micro Lett.* **2015**, *7*, 219−242.
(50) Simon-Deckers, A.; Loo, S.; Mayne-L'Hermite, M.; Herlin-Boime, N.; Menguy, N.; Reynaud, C.; Gouget, B.; Carriere, M. Size-,

https://dx.doi.org/10.1021/acs.chemmater.0c03969
Chem. Mater. 2021, 33, 1571−1580

Composition- and Shape-Dependent Toxicological Impact of Metal Oxide Nanoparticles and Carbon Nanotubes toward Bacteria. *Environ. Sci. Technol.* **2009**, *43* (21), 8423−8429.
(51) Wang, L.; Hu, C.; Shao, L. The Antimicrobial Activity of Nanoparticles: Present Situation and Prospects for the Future. *Int. J. Nanomed.* **2017**, *12*, 1227.

https://dx.doi.org/10.1021/acs.chemmater.0c03969
Chem. Mater. 2021, 33, 1571−1580